Finite element based modelling of the structural response of welded materials in complex loading configurations. Part II: Structural modelling considerations

A.J. Awang Draup[a,*], B. Rodgers[a], J.D Robson[a], P.B. Prangnell[a], Q.M. Li[a], M.J. Lunt[b]

[a]*The University of Manchester, Manchester, M13 9PL, UK*
[b]*DSTL, Porton, SP4 0JQ, UK*

Abstract

This three-part article presents a functional methodology for the inclusion of complex mechanical property distributions, which arise from microstructural variation due to welding techniques, into large scale structural models. The purpose of this is to enable a detailed study of deformation strain evolution of welds under complex loading to be modelled accurately, as this is often linked to failure. Part I details the interrelationship between microstructure and mechanical properties in 2139-T8 aluminium alloy, along with the methods for estimating the complex distribution of properties post-welding. In Part II, the effects of the inclusion of complex mechanical property distributions in finite element (FE) based simulations of laboratory scale structures is evaluated against the common techniques for modelling welds. Part III details the application of the verified coupled microstucture-FE technique to large scale welded structures subject to explosive blast loading. The combined studies demonstrate the importance of including microstructural effects in structural modelling for reducing the conservatism; this is particularly relevant when assessing ageing structures under severe fault conditions.

Keywords: Blast loading, Digital image correlation, Materials modelling, Finite element simulation, Materials characterisation

1. Introduction

The typical method to assessing structural response to external loading is to use the finite element method (FEM) and there are many instances of its use to study the response of welded structures [1, 2, 3, 4]. However, successful macro scale modelling of weld behaviour under general loading conditions is extremely challenging as there are many factors which contribute to the overall structural behaviour. In addition to the variation in mechanical properties across the weld zone, phenomena such as geometry misalignment from the welding process, the formation of weld defects, and residual stresses are all complexities which affect structural performance [5, 6], *e.g.* the adverse effect of residual stresses on fatigue life. Moreover, appropriate application of modelling techniques, such as definition of the mesh, external loads, and boundary conditions is pertinent to overall quality of predictions. Whilst there has been a lot of work to improve FE based modelling methods with respect to some of the afore mentioned phenomena [7, 2, 1, 8], a systematic approach to implementing local material property variation which arise due to welding process has not emerged in the public domain.

In FE based modelling, meso-scale complexity arising from mechanical property variation, is typically dealt with by partitioning the structural mesh into distinct regions that are suitably representative of the weld regions, e.g. Nugget, TMAZ, HAZ and parent material of friction stir welds [2, 1]. Elements of the mesh within these partitions and are collectively assigned homogeneous isotropic properties. It is common to only include variation in yield stress within structural models , which is normally assumed to scale linearly with hardness. The geometry of each region, such as the HAZ, may be defined by examination of the hardness distribution in the cross section of an actual weld or by visual inspection of metallographic specimens. However, it is common practice to calibrate the geometry of the model to experimental data from a real weld loaded in uniaxial tension. Usually, the calibrated model is extended to more complex structures and loading configurations without any further modifications [2, 6]. This approach will hereby be referred to as the "lumped-mass" method.

It is widely known that in reality, there can be local variation to thermal and strain rate sensitivity or work hardening rate

*Corresponding author. Tel: +44 (0)161 306 3578 Ext. 2261
Email address: jefri.draup@manchester.ac.uk (A.J. Awang Draup)

across the weld region [6, 9]. Since most weld models only account for yield stress variation across the weld important variation in material properties are neglected. As a result, strong material property gradients, which can be diffuse in nature, are over simplified when implementing step functions through the use of the lumped-mass method [2, 6]. Further, important material property gradients across the weld, in particular the work hardening rate are ignored. These simplifications make it difficult to obtain good matching between the predicted non-linear structural response and experimental data, local to the weld zone. Careful calibration of the partitioned zones is required in order to match the global non-linear response of the weld [2, 6]. Moreover, it is unclear whether a model calibrated to a particular loading condition, specifically uniaxial tension, will accurately describe the structural behaviour under more complex loading conditions, such as blast loading of a plate. Data in the public domain reveal that structural models using the lumped-mass method only appear to show good qualitative correlation of structural behaviour of complex models calibrated to a more fundamental loading configuration; any supporting quantitative correlation is not reported [2, 6].

1.1. Suitability of the lumped-mass method

Despite this known link between microstructural variation and mechanical properties, in many studies where the material property variation across the weld is explicitly modelled, all available evidence suggests that the local distribution is only resolved coarsely in each of the models [2, 1, 4, 7, 3, 5, 10]. The effect of using the lumped-mass method has not specifically been studied in the literature and shall be reviewed here. In some cases, the lumped-mass method can be representative of the properties across the weld, such as in non age-hardenable aluminium alloys subjected to FSW or fusion welded steels [11, 3]. As shown by Sato et al. for 1xxx and 5xxx alloys, the variation in both microstructure and mechanical properties is distinct across the weld. There is a distinct variation in the TMAZ and again in the nugget, which is related to the distinct variation in the contributions to alloy strengthening in those regions. Therefore, in these cases, a discrete meso-scale distribution of mechanical properties in the elements is a reasonably accurate description of physical reality. Moreover, this technique also requires a relatively small amount of computer memory as there are effectively only four material models to be referenced across the weld zone.

However, as noted by McWilliams et al. [2], for age hardenable alloys, there are strong gradients in both yield stress and work hardening rates across the weld zone, which is linked to local microstructural variation [12]. In their study conclusions, the authors mention that ideally, element-wise variation in yield stress would be a more appropriate way to specify material properties. This would enable accurate representation of the meso-scale yield stress variation across the weld. However, McWilliams et al. rightly point out that local work hardening response also demonstrates gradients across the weld, but that it does not scale simply with hardness. Additionally, specifying an element wise distribution of properties is a non-trivial task as most software is designed to assign groups of elements distinct properties [13]. Hence, specifying property distributions must be done either manually or via the use of a user defined sub-routine, which is a complex task, particularly when dealing with complex geometries. Furthermore, this method is likely to utilise a greater amount of computer memory because the number of constitutive models would relate to the element density, hence, the active variables stored in computer memory during each time step will be large.

As mentioned previously, the geometry of the weld regions are normally calibrated such that the global response of the weld matches an experimentally measured global response [2, 6]. As a consequence, the geometric size of defined regions do not accurately represent the observed geometry of the weld region. Hence, the using calibrated forms of the lumped-mass method impose that the meso-scale microstructural similarity between the weld region of the model and real specimen is neglected at the expense of overall structural response and geometry. Hence, it is unclear whether or not these models are suitable for studying localised effects within the weld region under loading [2, 6].

1.2. Consequences of the lumped-mass method

In conjunction with a fundamental understanding of the FEM, two major observations of the effect of the lumped-mass method on numerical prediction of strain distribution for studies in the public domain can be made. Firstly, this method appears to lead to severe discontinuities in strain at the interfaces of the macro scale weld zones (i.e. HAZ, TMAZ, etc.). Secondly, an artificial double strain localisation is predicted to occur in the weld under uniaxial loading conditions. The occurrence of the severe strain discontinuities can be explained by considering the property change in the elements, as shown in figure **??**. On the left hand side, the elements are assigned a relatively high yield stress, whereas the elements on the right are assigned a relatively low yield stress. Both sets of elements share a set of com-

mon nodes, which induces an artificial constraint on the elements with lower yield stress. Under loading, the elements with higher yield stress will deform slightly due to Poisson contraction under loading, whereas the elements with lower yield stress will deform more easily. However, at the interface the shared nodes are constrained to deform with the elements of higher yield stress. Effectively, the elements on the right hand side will demonstrate higher stiffness as they cannot deform as they would in reality [13]. Hence, it is possible that the solution in the region of interest is significantly affected by this constraint. Moreover, an increasingly fine mesh size is likely to exacerbate the effect because smaller elements are more sensitive to nodal displacement. This problem is intrinsic to the FEM and can be mitigated by minimising the mismatch in properties at the interface. This gives further support to the proposition to specify element wise yield stress variation by McWilliams et al. Figure 1 shows the predicted strain distribution in a welded sample in comparison to the experimentally measured strain distribution by McWilliams et al. [2] Quite clearly, at the boundary of the weld region interfaces, there is a significant discontinuity in plastic strain; similar effects are presented by Zadpoor et al. [7] Genevois et al. [9] also utilise the method but appear to obtain close correlation between simulation and experimentation, however, the authors only present midpoint values for strain distribution predicted by FEM in comparison with their high resolution DIC measurements. It is unclear whether or not the authors results would provide good matching, particularly at the weld interface.

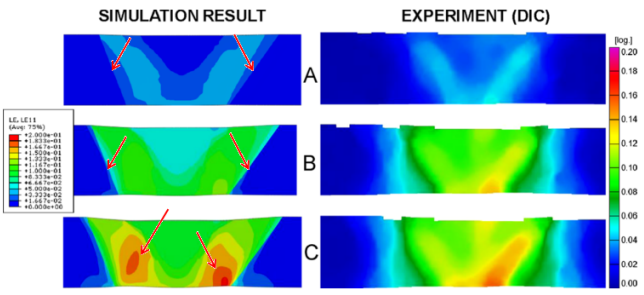

Figure 1: The simulated strain prediction for FSW 2139-T8 loaded in uniaxial tension across the weld using the lumped mass method. Figure also shows the experimental measured strain measurements using DIC at the start, midpoint, and end of the test. There is a severe discontinuity in strain predicted at the boundaries of the weld zone and the simulation also predicts double strain localisation either side of the weld centreline, which does not occur in reality. Figure adapted from McWilliams et al. [2]

With respect to the double strain localisation effect, figure 1 illustrates the development of strain either side of the weld centreline. It is unclear why this effect occurs given that the model was asymmetric about the weld centreline, but it is possibly associated with the artificial constraints placed on the elements within narrow regions of the weld. By definition, any model which assumes weld symmetry or symmetric boundary conditions will generate double strain localisation either side of the weld. The predicted behaviour is likely to be erroneous and most experimental evidence shows that , under tensile loading, strain localisation and necking only occurs in one side of the weld [14, 9] [14, 15, 12, 16, 9].

In contrast, the double strain localisation effect can be seen in experimental evidence but only during the forming of Taylor welded blanks [4, 5, 10]. It is possible that this phenomenon is linked to the stress conditions, which in the forming of sheets is approximately bi-axial. Under compound loading, materials that demonstrate yielding according to the Von Mises criterion, which is an assumption usually implemented in commercial finite element software [13, 17], can support loads greater than the uniaxial yield stress. Hence, it is possible that where material would normally yield on one side of the weld during uniaxial tension, due to the constraints imposed under biaxial loading, greater stresses are supported throughout the weld, thus, large strains can localise either side of the weld centreline.

In all studies reviewed here, highly detailed weld models were generated in order to assess structural failure or to implement mechanistic (micro-void growth and coalescence) models of failure into welds. However, the meso-scale mechanical property variation intrinsic to welds was only implemented at a much coarser resolution than other geometric details using the lumped-mass method. Given that the application of the lumped-mass method within the FEM is likely to induce erroneous local strain predictions, and only appears to provide correlation with experimentally measured strain distribution with the centre of the homogeneous weld regions, it is unclear whether or not the attempts by authors to incorporate complex anisotropic behaviour [5, 10] or mechanistic failure models [18] will provide an objective understanding of the failure of welds under loading, as fracture is strongly linked to plastic strain history at any given point.

1.3. Summary

The lumped mass method is a common technique for simplifying the complex distribution of material properties in FE models of welded structures; the method is used when studying localised damage effects in structures under loading. How-

ever, the method can be seen to lead to observable errors in predicted strain distribution, which has potential impact on numerical studies using it to assess localised damage in welds. The errors are linked to the fundamental theory of the FEM, and it is known that minimisation of these errors can be achieved by including element wise variation in material properties; this is a non-trivial task. The remainder of this paper is dedicated to observing the effects of the lumped-mass method and demonstrating the experimentally validated benefits of incorporating element wise complex property distributions in FE models of welded structures under loading.

2. Finite element modelling

Numerical modelling and simulation of welded panels was carried out using the commercial software package LS-DYNA version 971. In this study, the structural performance of welded material in loaded in uniaxial (cross weld) tension. The dynamic response of the structure was analysed using explicit time integration methodology. A displacement-based (Lagrangian) finite element analysis based on the virtual work principle was used to model the equations of motion. By integrating the equations of motion through time, the conditions within a discretised model of the system were determined. In particular, the nonlinear evolution of plastic strain across the weld region was of interest as it is linked to failure [**?**].

2.1. Model Geometry

In this study, 1:1 scale models of the experimental apparatus were built manually using HyperMesh (Figure 2). For all simulations, the welded structures were assumed not to contain any weld defects, such as porosity, kissing bonds, or root defects. Furthermore, it was assumed that there was neither misalignment of geometry arising from the welding process, nor any local weld flash. These assumptions were appropriate as care was taken to ensure samples were properly aligned during the welding process and the samples were machined to final geometry before testing. In all cases, 8-node solid hexahedron elements were used. In the weld region, the element mesh had a resolution equivalent to 1x1x1 mm.

2.2. Material Properties

For all modelled parts, Johnson-Cook material models were used to define plastic behaviour accounting for strain rate and thermal sensitivity. In the region of the weld (where the local mesh resolution is 1x1x1mm) each element in the weld cross

Figure 2: Example finite element mesh that was generated using the method in §2. Each colour code is indexed to a unique Johnson-Cook material modelled interpolated for the centroid of that element. The figure also highlights the node sets with boundary conditions specified in §2.4

section is assigned a unique Johnson-Cook material model. This allows strong gradients of material properties to be defined across the weld. For each unique material model, the parameters for equation **??** are defined based on the local thermal history, the post-weld hardness of the weld to be modelled, and mechanical property measurements obtained from "simulated weld material", as indicated by equations 1-5. By taking hardness measurements from three through thickness locations across the cross section of the weld in §3.2, a map of hardness at the centroids of each element in the mesh can be interpolated from theses measurements, and used to define the meso-scale geometry of the weld since hardness is an indicator of $\mathrm{f}_i(T,t,\vec{\mathbf{x}})$ in the weld. Simulated weld material is generated by heat treating parent material using equivalent thermal cycles for positions locally across the weld using a methodology described by Shercliffe [19, 20]; this method can also be used to predict the post-weld hardness of a weld [21, 22], which would allow prediction of weld structural response accounting for the welding parameters. Material property definition and, thus, meso-scale weld geometry is calibrated to a normalised weld condition rather than a particular loading configuration using this method, as is the case using the lumped-mass method. The Johnson-Cook parameters are shown to vary across the weld and are linked to changes in strengthening mechanism in response to the welding process. Further details of this method and experimental evidence for the link to strengthening mechanism variation are outlined in Part II the companion paper. An example of the parameters used to define material models for the elements across the weld cross section at the mid thickness of the plate are illustrated in figure 3.

$$A = k * Hv \tag{1}$$

$$B = \mathrm{f}_1(T,t,\vec{\mathbf{x}}) \tag{2}$$

$$n = \mathrm{f}_2(T,t,\vec{\mathbf{x}}) \tag{3}$$

$$C = \mathrm{f}_3(T,t,\vec{\mathbf{x}}) \tag{4}$$

$$m = \mathrm{f}_4(T,t,\vec{\mathbf{x}}) \tag{5}$$

Where

$$k = \mathrm{f}_5(T, t, \vec{\mathbf{x}}) \tag{6}$$

and $\vec{\mathbf{x}}$ is the position of the element centroid within the welded sample; details are provided in Part II.

2.3. Loading Considerations

The presence of welding induced residual stresses has been neglected as it is assumed that they are relieved either during specimen preparation, when samples are sectioned from the welded plate, or during the initial stages of loading [23]. Moreover, implementation of a representative residual stress profile in FSW 2139-T8 [6] in the modelled scenarios demonstrated negligible influence on the structural performance of the welds, though these have been omitted for brevity. Typically, residual stresses have influence over the propagation of cracks, and, hence, fatigue life of a structure rather than the deformation behaviour under loading [24].

Loading due to gravity was ignored as these are small in comparison to the applied load and therefore unlikely to significantly affect the structural performance of the welds. Loading on the specimens was not explicitly defined using an applied external force, rather it was defined via the use of boundary conditions as detailed in §2.4.

2.4. Boundary Conditions

In the models of welds loaded in uniaxial tension, the nodes at the ends of the specimen were assigned a prescribed motion boundary condition (`*BOUNDARY_PRESCRIBED_MOTION` input card). The boundary conditions are illustrated in figure 2, and for the node set NS10001, the velocity is set to $u = 0$ mm min^{-1}, whilst for the node set NS10005, the velocity is set to $u = 1$ mm min^{-1}. This is equal to the velocity of the moving cross head on the tensile rig.

3. Experimental Methods

In order to test the validity of the modelling methods described in the structural performance of welds under uniaxial loading was measured experimentally. The details of all the experimental methods used are presented below.

3.1. Welding parameters

2139-T8 plates were supplied from Constellium and all welding was carried out with the plates in the as-received condition. Samples were rigidly clamped and were positioned in direct contact with a steel backing plate.

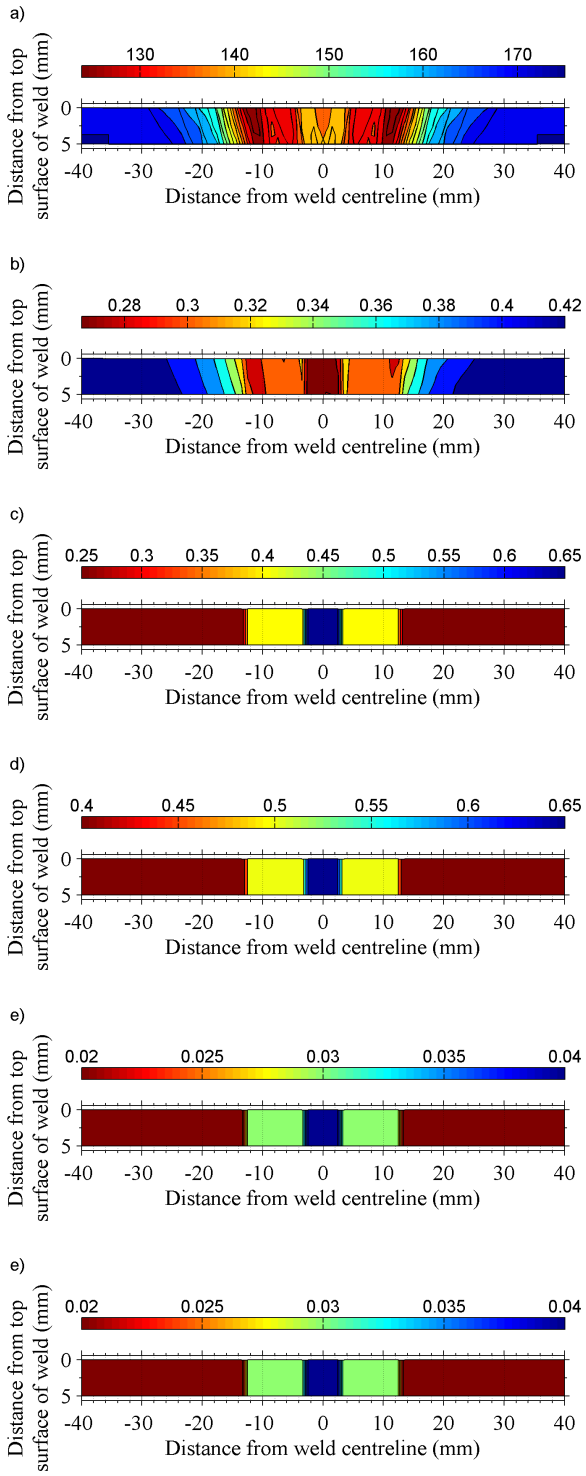

Figure 3: Element-wise distribution of properties interpolated across the weld cross section. a) Vickers Hardness b) Johnson-Cook A parameter (GPa). c) Johnson-Cook B parameter (GPa). d) Johnson-Cook n parameter. e) Johnson-Cook C parameter. f) Johnson-Cook m parameter.

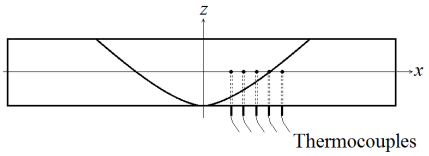

Figure 4: Schematic illustrating the position of thermocouples within the weld cross section.

Plates were machined into a work-piece with dimensions 150 mm x 300 mm x 6.38 mm (RD x TD x ND). The work-piece was machined with pilot holes to allow thermocouples to be embedded within; this enabled the thermal history within the work-piece to be recorded during the welding process. The thermal data was utilised to validate the post-weld hardness model (§**??** chapter **??**). Thermocouples were positioned at the centre of the plate (150 mm in RD) at a fixed depth, in the *z*-direction (3 mm in ND), from the top surface of the plate and at increasing distance from the weld centreline (0 mm, 3 mm, 5 mm, 8 mm, and 12 mm in TD) *x*-direction, as shown in figure 4.

Welding was carried out with a conventional tool featuring a tri-flat tapered pin. The tool dimensions were: 18 mm shoulder diameter with a 2 °concave angle, 5.8 mm pin length featuring a pin root diameter of 6.2 mm and a pin tip diameter of 4.5 mm. Welding was carried out with a rake angle of 10 °, tool rotation speed of 1000 RPM and a tool advance speed of 100 mm·min^{-1}. The initial plunge speed was set to 10 mm·min^{-1} and a dwell time of 10 s, whilst the tool extraction speed was set to 10 mm·min^{-1}. In total, a weld of 200 mm length was carried out parallel to RD. The measured average tool downforce was approximately 20 kN. Welding was carried out by the University of Manchester with a Crawford-Swift FSW machine with the tool in position control mode.

3.2. Tensile Tesing of FSW 2139-T8

Square cross section bars with dimensions 5x5x150 mm were machined from the welded plates. By preparing samples in this way, geometry induced stress concentrations arising due to weld flash are eliminated as they are milled away. Further, residual stresses are relieved as the specimen is no longer constrained by the bulk material. This also simplifies the modelling process and allows the effects of material property gradients to be isolated during tests. Samples were tested using an Instron 5569 machine where the cross-head displacement rate was set to 2 mm·min^{-1}. Testing was carried out according to BS6892-1:2009.

3.3. Digital Image Correlation

2D Digital Image Correlation (DIC) [25] was performed on square bar tensile specimens which captured the full weld region in order to measure the strain response of the weld. A LaVision Imager Pro Plus 4M greyscale camera, fitted with a Nikon AF-D Micro-Nikkor 105 mm f/2.8 macro lens and a Nikon 2x teleconverter, was used to acquire images with a 2096x2096 pixel resolution at a frequency of 1 Hz. The test setup was illuminated using a 150 W halogen lamp positioned at a low angle to the sample to avoid direct reflection into the camera.

The specimens were prepared for DIC by first systematically grinding the face of the sample to be imaged down to P180-P1200 grit. This ensures that the sample is flat, as required for 2D DIC, and has enough surface roughness to allow good adhesion between the paint and the sample surface. The surface was then thinly coated with a matte white surface primer; this prevents direct reflection of light into the camera. The sample was allowed to cure for 24 hours and was subsequently partially coated with a matt black spray paint. By partially coating the specimen, a unique speckle pattern forms naturally on the surface which can be analysed by the DIC software. The typical speckle feature size of the samples was approximately 3x3 pixels. DIC analysis was carried out using the commercial software package LaVision DaVis 8.1.5. A 2D time series cross correlation was carried out in integral mode using the sum of differential vector fields. Displacement calculation was performed with multi-pass iterations where the window sizes decrease from 128x128 pixels to 32x32 pixels. The final window had a circular Gaussian probability function fitted to the sub-regions to account for large strains and rotations; all subregions were located with 25% overlap.

4. Results

The relevant results and supporting discussion are split with reference to the particular loading condition studied. In particular, the focus of prediction and validation techniques pertains to the spatial and time evolution of plastic strain distribution across the weld. It is widely known that failure in ductile materials is often linked to the local plastic strain. In ductile materials, failure mechanisms such as formation of micro-voids, void coalescence and crack formation are heavily linked to plastic strain. Whilst there are many modelling methods which aim to predict these particular phenomena, they are not the focus of this study. The primary aim of the uniaxial tension study is to verify the prediction of strain distribution made using the

modelling method in §**??**; the precise determination of failure is not considered. The primary aim of the blast loading study in §**??** is to verify that the modelling method in §**??** accurately captures the strain evolution when extended to complex loading configurations. Again the precise determination of failure is not considered.

4.0.1. Experimentally measured strain distribution

On a macro scale, the evolution of axial strain is illustrated in figure 5a; the associated global stress-strain curve with positions $t_1 - t_5$ is shown in figure 6. It should be noted that there is a discrepancy in the overall measured initial yield stress and the prediction. Initial yielding is assumed to be controlled by the weakest region of the weld, i.e. the TMAZ/nugget. The discrepancy in figure 6 is consistent with the observed scatter in nugget data presented in figure **??**, chapter **??**.

In the early stages of global deformation, t_1, there is a relatively uniform distribution of strain all over the weld cross section. The strain distribution is $\leq 0.5\%$ in the z-x plane, though there are localised regions of fluctuating strain. At the onset of plastic deformation within the weld, t_2, the strain distribution begins to localise in the TMAZ, just outside the nugget region. The strain distribution is approximately symmetrical about the y-z plane and peak axial strain measures $\leq 5\%$ strain in the z-x plane. As global deformation continues, at t_3, axial strain remains approximately symmetrical about the y-z plane but is predominantly accommodated within the inner regions of the weld, i.e. the inner HAZ, TMAZ, and nugget. Axial strain is measured to be increasing towards the centre of the weld and is greatest within the nugget; peak axial strain measures $\leq 6\%$ in the z-x plane. At the onset of necking, t_4, axial strain begins to localise on the advancing side of the weld, approximately at the interface between the inner and outer HAZ. The strain distribution is no longer symmetrical about the y-z plane and peak axial strain is measured to be $\leq 17\%$. Just before the point of failure, at t_5, axial strain is localised completely within the necked region of the specimen. Overall, the peak axial strain is measured to be $\leq 40\%$ in the z-x plane.

On a local scale, the mid thickness axial strain distribution is shown in figure 7a. During the early stages of deformation, axial strain is measured to be approximately uniform over the entire sample, and is approximately $\leq 1.5\%$ between $|x| \leq 40$ mm. As global deformation continues, strain begins to increase over a progressively wider area of the HAZ, TMAZ, and nugget, and is approximately symmetrical about the centreline of the weld; the distribution of axial strain in this region is increasing to-

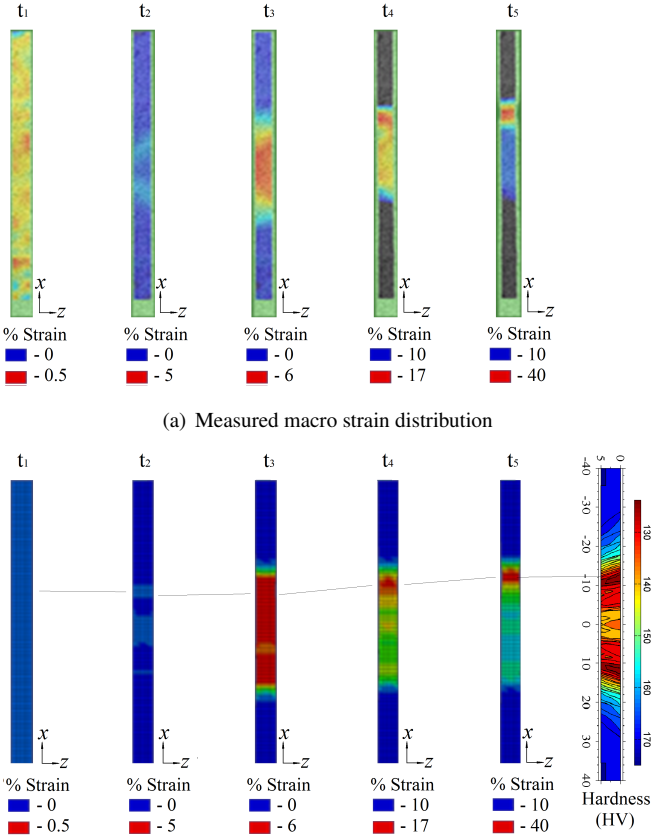

(a) Measured macro strain distribution

(b) Predicted macro strain distribution

Figure 5: Macro scale axial strain distribution taken at increasing time steps, transitioning the early stages of deformation to the latter stages of testing. a) Axial strain distribution measured experimentally using DIC. b) Axial strain distribution predicted using optimally defined mechanical property distribution (see details for simulation 9 in table **??**). The time steps equate to the equivalent global deformation steps between the ends of the specimen.

wards the centre of the weld. This trend continues until a critical moment in global deformation, where strain begins to localise at approximately $x = -12$ mm, on the advancing side of the weld. At the critical point, the strain distribution is approximately symmetrical and is confined within the region defined by $|x| \leq 20$ mm. Axial strain measures 15% in the region $|x| \leq 6$ mm. Beyond the critical point, the strain distribution remains approximately constant, except at $x = -12$ mm, where it begins to increase to the point of failure. At the end of the test, axial strain at $|x| \geq 20$ mm is $\leq 1.5\%$; axial strain increases rapidly from $x = -20$ mm to a peak of 22% at $x = -12$ mm; axial strain decreases to a plateau measuring 15% between $|x| \leq 7$ mm; axial strain decreases between $x = 7$ mm and $x = 20$ mm.

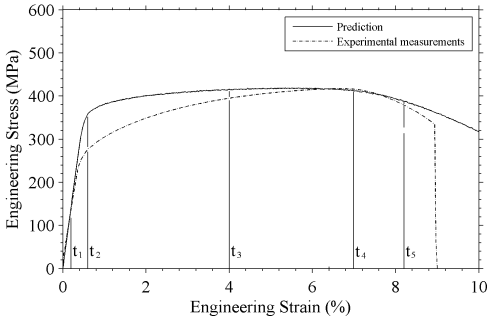

Figure 6: Predicted and experimentally measured nominal stress-strain curve plotted with the positions t_1-t_5 marked in figure 5..

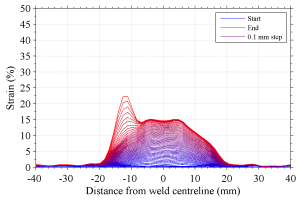

(a) DIC measured strain

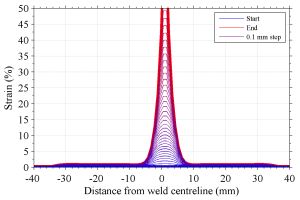

(b) Simulation 1: Hv-step, *k*-constant, *n*-constant

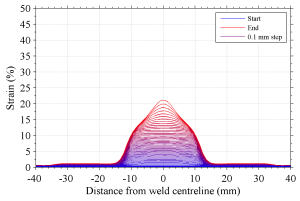

(c) Simulation 2: Hv-step, *k*-constant, *n*-constant

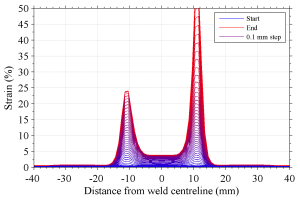

(d) Simulation 3: Hv-step, *k*-constant, *n*-constant

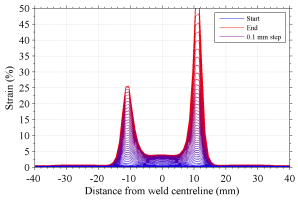

(e) Simulation 4: Hv-step, *k*-constant, *n*-step

Figure 7: Predicted strain distributions based on the lumped mass method. Strain distribution are plotted for every 0.1 mm of global deformation between the ends of the samples. Predicted strain transitions from blue, at the start of the test, to red, at the end of the test. Failure was not incorporated. Note that values of k, B, and n can be found in figure **??**c-e.

4.0.2. Simulations based on the lumped mass method

Simulations 1-4 (figure 7b-e) to show the effects of the lumped mass method, applied both directly and in calibrated forms, on the predicted strain distribution in the weld. In simulation 1 (figure 7b), the size of the weld zones correlate directly to those observed via optical macrograph. In simulation 2 (figure 7c), the weld zones are adjusted to capture key features from the hardness distribution of the weld, i.e. the minima in the hardness profile. In simulation 3 (figure 7d), the weld zones are the same in simulation 2 except that the width of the hardness minima is increased in order to better capture the material properties of the region containing the hardness minima. In simulation 4 (figure 7e), the weld zones are kept the same as in simulation 3, however, some variation in plastic response is allowed following the method by Genevois et al. [9]. This represents the state of the art in terms of current weld modelling techniques adapted from the lumped mass method.

In comparison to the experimental measurements, we can observe that application of either direct or calibrated forms of the lumped mass method all lead to significantly different behaviour. In simulations 1 and 2 (figure 7b-c), the methodologies do capture the initial yielding within the nugget region. However, deformation strain remains contained within the nugget region through the length of simulation in either model. The only observable difference is that in simulation 1, deformation strain remains confined to the narrow region of the TMAZ/Nugget, whereas in simulation 2, deformation strain is accomodated over a wider region of the weld. Unlike in the experimental observations, in both simulation 1 and 2, the predicted deformation strain does not transition out of the nugget region. Strain localisation is predicted to be in the centre of the nugget rather than in the position coincident with the hardness minima, as observed in experiment. It must be noted that the predicted response remains symmetric in simulations 1-2, which is consistent with the way the model is initialised.

In contrast, simulations 3 and 4 (figure 7d-e) demonstrate a consistent, almost identical, overall response. That response differs, markedly, from simulations 1-2 and the experimental results. The simulations do capture the initial yielding in the nugget region, however, deformation transitions rapidly into the regions either side of the weld centreline associated with the location of the hardness minima. Whilst a transition in the geometric distribution of deformation strain is captured in the simulations, the overall distribution does not correlate with experimental observations. Deformation strain is confined within these two narrow regions either side of the weld centreline throughout the simulation; this is consistent with the double strain localisation effect discussed in chapter **??** §**??**. It must also be noted that despite the models being initialised as symmetrical, the predicted response is asymmetric. In one of the regions

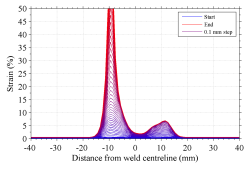

(a) Simulation 5: Hv-smooth, k-constant, B-constant, n-constant

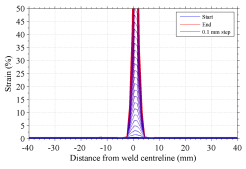

(b) Simulation 6: Hv-smooth, k-smooth, B-constant, n-constant

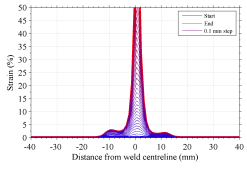

(c) Simulation 7: Hv-smooth, k-step, B-constant, n-constant

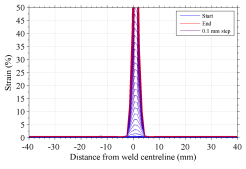

(d) Simulation 8: Hv-smooth, k-step, B-smooth, n-smooth

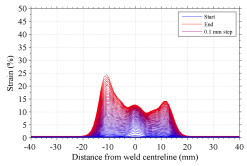

(e) Simulation 9: Hv-smooth, k-step, B-step, n-step

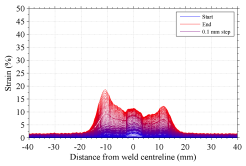

(f) Simulation 10: Hv-smooth, k-step, B-step, n-step

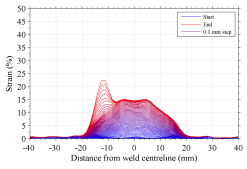

(g) DIC measured strain

Figure 8: Predicted strain distributions by systematically varying the yield stress and plastic behaviour. Strain distribution are plotted for every 0.1 mm of global deformation between the ends of the samples. Predicted strain transitions from blue, at the start of the test, to red, at the end of the test. Failure was not incorporated. Note that values of k, B, and n can be found in figure **??**c-e.

associated with the hardness minima, deformation strain is predicted to be greater than on the other side.

4.0.3. Simulations based on the method developed in the present chapter

Simulations 5-10 systematically demonstrate the effects of modelling method developed in the present chapter. Simulation 5-7 show the effects of the yield stress distribution, as influenced by the variation in relationship between hardness and yield stress (k-parameter). Simulations 7-9 show the effects of the plastic response, as defined by the upper and lower bound distributions of the B and n-parameters. Simulation 10 is a numerical mesh convergence study demonstrating the stability of the numerical simulation method using the optimal property distributions, which are identified as those in simulation 9.

Simulation 5 (figure 8a) shows an initial yield yield response similar to the lumped mass method found in simulation 3 (figure 7d). Initial yielding occurs in the regions associated with the hardness minima, however, deformation strain is accommodated over a much wider region of the weld compared to the lumped mass method. Simulation 5 shows that strain distribution increases across the weld region with increasing global deformation, similar to simulation 3. However, in contrast to simulation 3, strain begins to localise on the side of the weld associated with the lowest hardness minima; simulation 5 does not exhibit a double strain localisation effect. Simulation 7 (figure 8c) shows a similar initial response to simulation 5, however, the overall increase in strain across the weld is lower. Moreover, final strain localisation occurs in the nugget instead of at the hardness minima.

In contrast, both simulation 6 (figure 8b) and simulation 8 (figure 8d) show initial yielding in the nugget region followed by strain localisation; deformation strain remains contained within the nugget throughout the length of the simulation. The predicted response in both these simulations is markedly different from the experimental results figure 8g).

Simulations 9 (figure 8e) and 10 (figure 8f) show a consistent response, which correlates reasonably with the experimentally measured result (figure 8g). Initial yielding occurs over the nugget region of the weld, and, under increasing global deformation, strain evolves over an increasing proportion of the HAZ. Eventually, plastic strain begins to localise at the location coincident with the hardness minima. The main difference between simulation 9 and 10 is that the absolute values of the plastic strain distribution across the weld are slightly lower with the refined mesh.

For simulation 9, the global strain distribution is presented in figure 5b; the associated global stress-strain curve with positions $t_1 - t_5$ is shown in figure 6. It is clear that the overall distribution correlates reasonably well with the experimentally measured strain in the weld cross section, as shown in figure 5a. It should be noted that a diffuse distribution of plastic strain is observed in the HAZ.

5. Discussion

In this discussion, focus shall be given to interpreting the predicted deformation response of the weld under loading in

comparison to the experimentally measured response. This enables the effect of the user input mechanical property distribution to be understood more readily. The discussion highlights some of the practical difficulties and limitations in both applying the lumped mass method and interpreting numerical predictions based on the associated assumptions. Furthermore, the discussion identifies some key requirements, in terms of defining complex mechanical property distributions, which are necessary for accurate and reliable predictions of the local strain distribution. Moreover, the discussion provides insight to the true distribution of mechanical properties within an actual weld, and its relationship with microstructure.

5.1. Interpretation of experimental results

From the experimentally measured axial strain distributions, on both a macro and more local scale, it is clear that initial yielding occurs across both the TMAZ and nugget. The measured local axial strain distribution suggests that axial strain maybe slightly higher within the TMAZ, though the distribution is relatively uniform over these two regions. Nevertheless, the observed initial yielding response is consistent with directly comparable experimental data presented by McWilliams et al. [2] Moreover, this observed initial response should be expected; the measured mechanical properties from representative weld material, as presented in §**??** chapter **??**, suggest that initial yield stress is lowest within the TMAZ/nugget region. It is useful to note at this point that despite the minimum hardness in the weld being within the HAZ, initial yielding occurs in the TMAZ/nugget region. This indicates that the *k*-parameter distribution decreases towards the centre of the weld, which is consistent with observations of the mechanical properties as estimated from the representative weld material presented in chapter **??**. This complex distribution of the *k*-parameter must, therefore, be an important consideration for accurate modelling of the non-linear weld response.

As global deformation continues, the flow stress increases in the bulk region incorporating both the nugget and TMAZ via work hardening. This enables the immediately surrounding region of the inner HAZ to yield and begin to accommodate deformation strain. This process continues with global deformation, enabling a progressively wider region of the weld to yield and accommodate deformation strain. Within the outer HAZ, the peak axial strain measured decreases gradually, or diffusely, with increasing distance from the weld centre. This response should be expected because local flow stress is dominated by the volume fraction of Ω phase, which decreases gradually towards the centre of the weld. The volume fraction is linked to the gradual dissolution of Ω phase in the weld [2, 1]; this process is a function of the peak temperature experienced during the weld thermal cycle [22, 26].

At the critical point, axial strain begins to localise at the position coincident with the location of minimum hardness in the weld, which can be interpreted to occur due to two reasons. Firstly, the bulk inner region of the weld (i.e. the region confined between both hardness minima) has a larger capacity for work hardening than the outer regions, as estimated from the representative weld material. This is important because it causes the flow stress of the inner region to increase at a faster rate than the outer regions, owing to the difference local work hardening response. The estimated stress-strain response predicted by the constitutive models of the representative weld material (table **??**) suggests that when the inner HAZ and TMAZ/nugget regions are deformed beyond approximately 10% plastic strain, the flow stress in the TMAZ/nugget and inner HAZ will be consistently greater than the flow stress in the outer HAZ; this is due to the difference in the work hardening response. More succinctly, the stress-strain curves of the inner HAZ and nugget/TMAZ cross over the stress-strain curve of the outer HAZ, as shown in figure 9.

Secondly, since there is a decreasing distribution in flow stress in the outer HAZ towards the centre of the weld, linked to the decreasing volume fraction of Ω phase, axial strain will be distributed such that it is increasing towards the weld centreline. However, the strain distribution but will be constrained by the mismatch in flow stress at the interface between the inner and outer HAZ (where the stress-strain curves cross over each other). Hence, the onset of strain localisation and necking occurs at the interface of the inner and outer HAZ. For 2139-T8, this position is coincident with the location of minimum hardness in the weld. As the mechanical properties of 2139-T8 are dominated by Ω, the hardness distribution represents a good indicator of final strain localisation, due to the characteristic mechanical property distribution within the weld cross section that are linked to the microstructure. However, the hardness minima cannot be assumed to define the probable failure location for a general precipitate hardened aluminium alloy. This is because the hardness distribution is not always unambiguously indicative of the local mechanical property distributions in the weld, particularly the plastic response of the weld regions. As mentioned in the literature review, under aged alloys, or alloys strengthened by a more than one dominant strengthening phase

have a more complex relationship with hardness.

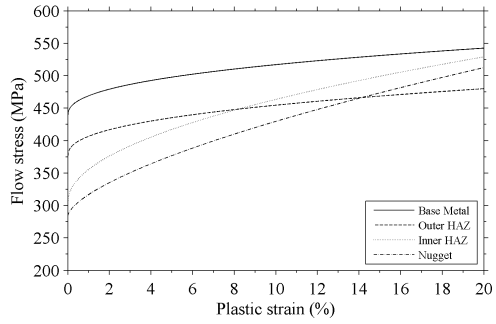

Figure 9: The plastic stress-strain response of the different local regions of the weld according to the Johnson-Cook parameters in table **??**. Note that the stress-strain curves of the inner regions of the HAZ and the TMAZ/Nugget cross over the stress-strain curve of the outer HAZ after a critical plastic strain; this is due to the difference in work hardening response.

The interpretation of measured strain distributions can be assumed to be reasonably accurate on a local scale, because DIC measurements following the method outlined in chapter **??** are estimated to provide strain measurements to an accuracy of $\pm 0.05\%$ strain [25]. The reliability of the method can be assessed by comparing the strain measurements to strain gauges or extensometers. Whilst, it is not presented here for brevity, the global engineering strain response was comparable to the response measured using an extensometer; the global engineering strains are $\pm 0.1\%$, for engineering strains of $\leq 15\%$, and $\pm 1\%$, for engineering strains of $\leq 20\%$. There is a divergence in correlation with extensometer readings at larger strains, however, the extensometer does not account for necking. It is more likely that the strain measurements are more representative of the actual response using DIC despite this apparent reduction in reliability, though this does depend on the coherency of the paint with the sample surface. Nevertheless, the interpretation of the experimentally measured response can be assumed to be fairly reliable. Moreover, the interpretation correlates with the estimated local mechanical properties and can be linked to the observed microstructural variation.

5.2. Interpretation of simulations based on the lumped mass method

As will be discussed here, practical application of the lumped mass method to FSW, whether direct or in a calibrated form, as described in the literature, is not straightforward and can lead to complications from both a metallurgical perspective and a numerical modelling perspective. There is a trade-off between the metallurgical similarity of the model with the actual weld and both the numerical accuracy and reliability of the predicted results. Using direct application of the lumped mass method, metallurgical similarity is promoted, whereas through a calibrated approach, numerical accuracy is promoted. In this section, the commonly used methods are discussed based on the results described in §**??**.

As mentioned in §**??** chapter **??**, under the lumped mass method, the weld region is partitioned into distinct regions, which are representative of the nugget, TMAZ, HAZ, and parent material. Partitioning is based on the hardness distribution and observation of macrographs of the weld cross section. The distinct nugget and TMAZ region are easily determined, geometrically, from the weld macrographs, and the unaffected zone can be identified from the hardness distribution. Homogenising the elements of the mesh into the four basic regions does make logical sense from a simplified metallurgical perspective, though it is dependent on welding conditions. However, as will be discussed, from a numerical modelling perspective, this is not always appropriate, as there are unintended consequences if the assumptions of the lumped mass method are applied exactly. As a result, calibrated forms of the lumped mass method are used to accommodate the effects of these assumptions. However, there are always limitations to the results, and care must be taken during interpretation of their validity, as shall be discussed here. As a reminder, the basic assumptions of the lumped mass approach are that: yield stress scales directly with hardness; the linear coefficient relating hardness to yield stress is constant across the weld; there is no variation in work hardening behaviour across the weld.

5.2.1. Calibration

Simulation 1 represents direct application of the standard lumped mass method, as described in chapter **??**. In this case, the widths of the bulk weld region, as defined by the hardness distribution, are representative of the weld cross section from a metallurgical perspective. However, as shown in figure **??**a, the minima of the hardness distribution across the weld is neglected even though it is the point associated with strain localisation. In addition, the plastic response across the weld is assumed to be equivalent to the parent material. From a numerical perspective, key regions of the weld are neglected from the model which are sources of error.

Simulation 2 represents a calibration of the standard form of the lumped mass method; the width of the nugget region has been artificially increased and also incorporates the TMAZ and

inner HAZ regions. The modelled TMAZ has become a narrow region associated with the minima of the hardness distribution of the weld, as shown in figure **??**a. In addition, the plastic response across the weld is assumed to be equivalent to the parent material. From a metallurgical perspective, this method is less representative of the weld cross section compared to simulation 1. However, the region incorporating the hardness minima is captured in the model, which is an improvement from a numerical perspective.

Simulation 3 represents further calibration to the lumped mass method in simulation 2; the width of the nugget region remains artificially increased to incorporate the TMAZ and inner HAZ. The width of the TMAZ region has also been increased (artificially) but remains associated with the minima of the hardness distribution of the weld, as shown in figure **??**b. The plastic response across the weld is still assumed to be equivalent to the parent material. From a metallurgical perspective, this method is less representative of the weld cross section compared to simulation 2. However, the relative importance of the region incorporating the hardness minima has incresed, which would serve to improve numerical accuracy of the simulation.

Simulation 4 represents further calibration to the lumped mass method in simulation 3, and is equivalent to the method used by Genevois et al. [9] to model the structural response of aluminium welds. The width of the nugget region remains artificially increased to incorporate the TMAZ and inner HAZ, and the width of the TMAZ region remains artificially increased and associated with the minima of the hardness distribution of the weld, as shown in figure **??**b. However, the plastic response across the weld is no longer assumed to be equivalent to the parent material and local plastic response is specified. From a metallurgical perspective, this method is as representative of the weld cross section as simulation 3. From a numerical perspective, there is additional information about the work hardening response which serves to improve the accuracy of the simulation.

It can interpreted that calibration of the lumped mass method is performed in order to achieve good correlation between the predicted and experimentally measured global stress-strain response of the weld. Nevertheless, exact details of calibration methods are typically omitted from studies in the literature. Calibration allows important features of the weld, such as the hardness minima, to be captured using the lumped mass method. Hence, calibration is a trade-off between metallurgical similarity of the numerical model with physical reality, and known key features of the weld. However, from figure 7a-e, it is clear that application of the lumped mass method, either directly or in a state-of-the-art calibrated form, is unsuitable for 2139-T8 alloy. There are significant differences between the predicted and experimentally measured strain evolution under loading. These differences manifest primarily in the initial yield response and the geometrical evolution of strain due to work hardening; these are discussed further in the following paragraphs.

5.2.2. Initial yield response

The user input hardness profile is directly indicative of initial yield response, since hardness and yield stress are assumed to have a linear relationship that is constant across the weld. Therefore, in simulations 1-4, the lowest theoretical yield stress is effectively in the TMAZ, followed sequentially by the nugget, HAZ, and parent material. It is expected, therefore, that the TMAZ yields first, and as it work hardens, the increase in flow stress will allow the elements associated with the nugget to yield and accommodate deformation strain. As the flow stress in the TMAZ and nugget increases via work hardening, the elements in the HAZ will begin to yield.

In contrast to the expected initial yield response, figure 7b-c (simulations 1-2) both show that initial yielding actually occurs in the elements associated with the nugget and that the majority of axial strain is accommodated within the nugget region throughout the entire simulation. The result suggests that the elements within the TMAZ are behaving as if they had a greater flow stress compared to the nugget region. As described in chapter **??**, the lumped mass method causes an artificial increase in the elemental stiffness at the partition of the weld zones. This effect is exacerbated by the low number of elements in the TMAZ across the weld (1) and is most pronounced in both simulation 1 and simulation 2. It also shows that in these important regions, which may be relatively narrow, an appropriately larger number of elements should be used to model the region in order to avoid errors in the numerical solution.

Therefore, the source of the numerical error can be traced back to the calibration stage, and is exacerbated by the assumptions in simulation 1 and 2. In simulation 1, the TMAZ is approximately 800 μm wide thus is represented by a single 1x1x1 mm element. In simulation 2, the TMAZ represents the region encompassing the hardness minima. Since the hardness measurements are taken at 1 mm intervals, the TMAZ is also represented by a single 1x1x1 mm. Hence, all the elements of the TMAZ share common nodes with the surrounding ele-

ments of the nugget and HAZ; these regions have a greater yield stress than the TMAZ itself. Thus, the elements associated with the TMAZ are constrained to deform with the surrounding elements, thereby demonstrating an artificial increase in elemental stiffness. Since the absolute difference between the assigned yield stress of the nugget and TMAZ is relatively small, the elements of the TMAZ do not yield first despite being assigned the lowest initial yield stress. These elements are shielded due to their increased stiffness, and deformation is confined to elements with the second lowest yield stress, i.e. the nugget.

In simulations 3-4, the problem of artificially increasing elemental stiffness is attenuated by increasing the effective width of the TMAZ during calibration. This procedure allows an increased number of elements to form part of the narrow TMAZ, hence, the inner-most elements are shielded from the artificially increased stiffness effect. Figure 7d-e show that initial yielding occurs in the elements associated with the hardness minima, and that deformation is subsequently accommodated in the elements of the nugget after work hardening, as expected.

5.2.3. Non-linear response

Generally, in the lumped mass method, work hardening variation in the weld is ignored, however, it can be included as part of the state-of-the-art lumped mass approach. Neglecting work hardening variation is a conservative simplification that is applied to speed up the modelling process. As described in §5.1, the distribution of work hardening properties is responsible for causing geometrical evolution of strain distribution and strain localisation before failure. It is reasonable to suppose that all models neglecting the work hardening property distribution would not demonstrate this geometrical evolution of strain (i.e. simulations 1-3) and vice versa (simulation 4). However, figure 7b-e all indicate that significant geometrical strain evolution does not occur either with or without the user input distribution of work hardening properties. The first observation here is that in simulations 1-4, the distribution of plastic strain post yielding remains geometrically consistent throughout the length of the simulation.

A second observation from simulations 3-4 is the evolution of two points of strain localisation, approximately symmetrically, about the weld centreline. This double strain localisation effect is caused by the symmetric initial distribution of plastic properties in the model setup. The flow stress is significantly lower in the TMAZ regions, and remains so throughout the simulation. Even with the inclusion of work hardening properties, as used in simulation 4, the initial yield behaviour dominates, and there is an insignificant effect on the simulated response of the weld. It should be expected that all simulations 1-4 should demonstrate this double strain localisation effect. However, in simulation 1-2, the predicted result is significantly influenced by the artificial increase in elemental stiffness within the TMAZ, as mentioned previously.

A third observation, from simulations 3-4, is that the lumped mass method appears to be numerically unstable at high deformation strains. In simulations 1-4, the models are all setup as symmetric problems in the x-axis. However, in simulations 3-4, the initially symmetric distribution of strain eventually transitions to become asymmetric. More succinctly, the prediction correlates with theoretical expectation for the majority of the simulation, but eventually diverges. The exact reason for this is unclear, and it is possible that the asymmetry may due to the different boundary conditions placed on the nodes at the ends of the tensile specimen. At one end, the nodes are fully fixed, whereas at the other end, the nodes are assigned a prescribed velocity in the axial direction, x. However, nodal translation and rotation remains constrained at all times, i.e. $R_x = R_y = R_z = y = z = 0$ and whilst $x \neq 0$ it is specified at all time steps. It is possible that this represents a numerical asymmetry in the PDE, however, the boundary conditions are assigned far away from the region of interest, and are chosen to minimise impact on the simulation. Moreover, the variation in flow stress assigned to the elements in the centre of the weld is more likely to dominate over the boundary conditions.

Alternatively, this asymmetry in predicted strain distribution may be due to a numerical instability, which occurs in elements with large strains. In the FE formulation, energy conservation is assumed within the elements. However, computation is dependent on the geometry of the element, which varies in time. As the element becomes skewed, or distorted at large strains, it has the potential to impact on the numerically calculated energy associated with the element. The FE software necessarily performs numerical truncation to values assigned to each element, hence, it is possible that at large strains, there is a small difference in elemental energies about the weld centreline imposed by numerical truncation that satisfies energy conservation in the system. This represents a numerical instability in the solution of the PDE via the FEM. Since the applied numerical methods used in commercial FE software are proprietary, the source of this cannot be identified unambiguously. It should be noted, however, that the instability occurs after strains of 20% are achieved in the weld. In reality, the material is likely to

have fractured before these levels of strain are reached, hence, the prediction is physically non-representative at such large deformation strains. Despite the model behaving as expected up to the onset of numerical instability, the overall prediction of strain distribution and evolution varies significantly from the experimentally measured response.

5.2.4. Implications for failure prediction

The calibration procedures in simulation 1-2 are not reported in the public domain for precipitate hardened aluminium alloys, to the best of the author's knowledge. Hence, greater focus will be placed on simulation 3-4.

The method in simulation 3 is used by Grujicic et al. [1] to predict the deformation in FSW 2139-T8. Following this method, no consideration to the work hardening response is incorporated, thus, the predicted local strain distribution is strictly non-representative and must be inaccurate. Grujicic et al. [1] further extend their calibrated model to study the response of a larger structure under more complex loading. It was found that failure was predicted to occur in a similar location as in the uniaxial simulations. This would be expected based on their calibration, though the reliability of the prediction is unclear as the study was purely numerical and not verified experimentally. The local stress strain conditions under complex loadings is likely to be different than in simple uniaxial tension, and it is not clear whether the calibrated weld zone would be representative under those conditions. It must be noted, however, that the main purpose of their numerical study was to assess an alternative method for homogenising the weld zones into the equivalent nugget, TMAZ, HAZ, and unaffected zone. The authors wanted to determine if a simpler approach for homogenising the weld zones affected the numerical prediction of failure. Given that both approaches result in weld zones which were similar, in terms of geometry and mechanical properties, it was unlikely that the predictions would be significantly different. However, the authors also incorporated a failure criterion to utilise the model for assessment of damage in complex loading. Given that failure is intrinsically linked to plastic strain in the simulation, and that the evolution of strain on a local scale is likely to be erroneous, as indicated by figure 7d, it is unclear if the assessment of failure by Grujicic et al. is reliable. It is unlikely that any study following this method can provide accurate quantitative description of local failure despite the ability of the method to provide good global correlation with experiments.

The calibration method in simulation 4 is applied by McWilliams et al. [2] to simulate the structural response of FSW 2139-T8 in uniaxial tension. After their calibration procedure, the modelled nugget remains geometrically representative of the weld, however, the relative size of the TMAZ is overestimated. In the model, it is approximately 5 mm in width, however, the macrograph of their weld indicates that the actual size is ≤ 1 mm. The size of their TMAZ is consistent both with Genevois et al. [16], who observe that extremely narrow TMAZ arise in precipitate hardened alloys, and the evidence presented in chapter **??**, where the TMAZ is observed to be $\leq 800\mu$m. Furthermore, in their model, McWilliams et al. explicitly ignore the HAZ, and homogenise it as part of the unaffected parent material. Whilst their model does provide close correlation with the experimentally measured global stress-strain response of the weld, the model has lost a large proportion of physical similarity with the metallurgical system. Moreover, their model leads to poor correlation on a local scale, as described in §**??** chapter **??**. The effects of their method include: double strain localisation either side of the weld centreline, stress shielding within the nugget, and the distinct strain discontinuity at the interfaces of the different weld regions. This effects are consistent with the results of simulation 4, as shown in figure 7e.

Genevois et al. [9] also use the same calibration procedure in simulation 4, however, they use directly measured mechanical response from the individual weld regions using DIC. Moreover, they further partition the HAZ region to account for more variation in yield stress and work hardening response across the weld. The presented response provides much closer correlation with experiment on a local scale. However, the predictions erroneously show that strain is greatest in the nugget at the end of the simulation, rather than in the region associated with the hardness minima. The reason for this is unclear, and is possibly linked to the distinct change in properties across the weld region, which may induce deformation strain to be accommodated in the central nugget region. Alternatively, these errors may simply be due to the fact that the majority of elements are assigned mechanical properties which are non-representative, in terms of yield stress and work hardening response, which dominates the predicted response despite inclusion of work hardening variation in the weld.

The evolution of plastic strain in the literature is consistent with the results produced in this study, which indicate that there is a high degree of uncertainty in the predicted response. In terms of predicting failure, which is linked to the local distribution of plastic strain, it is unclear that using any form of the lumped mass method will be reliable, based on the studies pre-

sented here. In addition, given the high degree of uncertainty in failure prediction in simple uniaxial loading conditions, the efficacy of extending a lumped mass model, which is calibrated under uniaxial tension, to model failure under complex loading remains questionable.

5.3. Interpretation of simulations based on the method developed in the present chapter

As discussed in the previous section, the lumped mass method induces intrinsic errors when applied to FE based modelling of welds; these errors are linked to the oversimplification of the true mechanical property distributions within the weld. The purpose of this complimentary study is to examine, systematically, the effects of including the complex distribution of local weld properties on the predicted strain distribution, using the method defined in §**??**. As will be discussed here, the study highlights some important requirements to successfully predict the local evolution of strain distribution. Moreover, the study will provide insight into the true distribution of mechanical properties, which could not be determined unambiguously from materials and mechanical property characterisation data.

As a useful reminder, simulations 5-7 allow the effect of local yield stress distribution to be assessed, whilst simulations 8-9 allow the effect of local work hardening response to be assessed; from these simulations, a set of optimal property distributions are identified. A mesh resolution study, simulation 10, was performed using the optimal property distributions to test the numerical reliability of the predictions.

5.3.1. Calibration

It is useful to remind the reader that, using the approach described in §**??**, the user no longer has to calibrate the size of each weld zone arbitrarily, as required by the lumped mass method. Instead, calibration is based on a metallurgical description of the weld only; the user is required to specify the loci defining the boundary between the inner and outer HAZ and the loci defining the nugget boundary. The former is based on a theoretical point of full softening, which is coincident with the hardness minima for 2139-T8, and the latter is defined by the geometry of the FSW tool probe. Each element of the weld cross section is assigned a unique constitutive model based on the local value of hardness, and the empirically estimated mechanical properties of the weld; both of these entities are found to have a characteristic distribution in the *z-x* plane, which is normalised to the precipitate dissolution response of the alloy and the local thermal cycle during welding.

As a result, a more detailed distribution of properties can be captured, thereby increasing the possibility of generating representative predictions of local strain distribution. However, the method is more resource intensive, and relies on an accurate description of the characteristic mechanical property distribution in the *z-x* plane; in this study the distributions are unknown and the simulated structural response is limited by the upper and lower bound property distributions. Moreover, the study is not practically achievable without automation of the process of generating input files for FE software.

5.3.2. Initial yield response

In all simulations, a linear relationship between yield stress and hardness is assumed alongside the use of a diffuse, or smooth, distribution of hardness. In simulation 5-7, the respective user input k-parameter distribution across the weld is either constant, smooth, or stepped. Collectively, the combination of k and hardness allows the diffuse distribution of initial yield stress is defined. Thus, across any element boundary, the relative difference in properties is minimised; theoretically, this attenuates the artificial increase in local elemental stiffness associated with the lumped mass method. The work hardening B and n-parameters, are assumed to be constant. Following this approach, for simulations 5, it is expected that initial yielding will occur in the elements associated with the hardness minima, and that as the flow stress increases via work hardening, the immediately surrounding elements will begin to yield and accommodate deformation strain. The region accommodating deformation is likely to be wider than in the lumped mass method (simulation 1), and as global deformation continues, axial strain will begin to localise in the regions associated with the hardness minima either side of the weld centreline. Since the user input hardness distribution is asymmetric, it is expected that deformation will eventually localise in the elements associated with the minima on the weakest side towards the end of the simulation, i.e. the advancing side of the weld.

Figure 8a shows that simulation 5 generates predicted results that correlate with the theoretically expected description above. Qualitatively, this indicates that the interpretation of the results is more reliable based on the approach developed in the present chapter, in comparison to direct application of the lumped mass method (figure 7b). This is because any induced numerical errors in the prediction do not dominate the predicted numerical response, which occurred following simulations based on the lumped mass method. This demonstrates that the artificial increase in local elemental stiffness, due to the

mismatch in mechanical properties at elemental boundaries, is indeed attenuated. Whilst artificial increase in elemental stiffness can never be eliminated entirely, as it is an intrinsic error associated with discrete models of a continuous system, the effect is significantly attenuated.

Quantitatively, it is difficult to assess the accuracy of the result (figure 8a) because local errors vary, both geometrically and temporally, in comparison to the experimentally measured evolution of strain distribution (figure 8g). The magnitude of local errors, compared to the experimentally measured response, are similar using the approach associated with either simulation 1 or 5. However, the region of the weld associated with the errors are different in either methods. By incorporating local yield stress variation, the output prediction is qualitatively similar to the predictions using the calibrated lumped mass approach (figure 7d-e). This indicates that the assumptions used in simulation 5 generate predictions which have accuracy and reliability that are at least as comparable to an optimally calibrated lumped mass method. The advantage with the present method is that the size of the weld zones is not arbitrarily set, thus, the method remains representative of the physical system from a metallurgical perspective. Moreover, the predicted asymmetry in the present simulation is not induced by a numerical instability, which is indicative that the symmetric assumption used in the literature limits the validity of the predictions using the lumped mass method. Whilst it must be noted that the instability following the lumped mass approach only occurs at relatively high strains, which are beyond the uniaxial fracture strains associated with most structural aluminium alloys, the critical strain at the onset of numerical instability (20%) is achievable for some alloys. However, it can be concluded that the inclusion of smooth distribution of hardness is beneficial for numerical prediction, as it captures the diffuse mechanical property variation in the HAZ more accurately.

Despite the improvements in numerical reliability from simulation 5, the location of initial yielding does not occur in the nugget regions, as measured experimentally (figure 8g). This suggests that the assumption that the k-parameter distribution is constant across the weld is limiting the predicted response. In simulation 6, the same input parameters as simulation 5 are used except that the k-parameter is allowed to vary assuming the lower bound distribution. Figure 8b (simulation 6) shows that, whilst initial yielding does initially occur in the nugget region, deformation strain is contained within the TMAZ and nugget region throughout the entire simulation. This could suggest that the initial yield stress assigned to the elements of the nugget and TMAZ regions is too low, which would lead to premature yielding and accelerate the strain localisation process. However, given that yield stress is linked to the empirically measured mechanical properties, which demonstrated close correlation with reported values in the literature, this is unlikely.

Since the initial yield stress is a function of the hardness and k- parameter, the distribution of both of these parameters affects the overall distribution of yield stress. The user input lower bound k-parameter distribution has caused the distribution of yield stress to decrease over a narrower region towards the centre of the weld, i.e. the initial yield stress distribution varies more severely than in reality. Effectively the initial yield stress distribution acts as a stress riser, or a notch, increasing the stress in the elements at the centre of the weld. Hence, after initial yielding, strain is forced to localise in the elements associated with the nugget region because the flow stress in the immediately surrounding elements is attenuated, i.e. the elements of the HAZ are shielded by the meso-scale stress riser caused by the mechanical property distribution. It can be assumed that the user input lower bound k-parameter distribution assigns the elements associated with the inner HAZ a higher initial yield stress than they actually have in practice. Thus, it can be concluded that the lower bound k-parameter distribution leads to an over prediction of the gradients in the initial yield stress distribution.

In simulation 7, the same user inputs are used as simulation 5 except that the k-parameter is allowed to vary assuming the upper bound distribution. Figure 8c (simulation 7) shows that initial yielding occurs over the nugget region. Moreover, deformation is distributed across the HAZ due to work hardening, and eventually strain localisation occurs within the nugget. This suggests that the effective stress riser, or notch, arising from the meso-scale distribution of initial yield stress, using the upper bound k-parameter distribution, is less severe than that caused by the lower bound k-parameter distribution, i.e. the distribution of initial yield stress varies over a wider region of the weld. This causes the elements associated with the nugget to yield first and local flow stress increases due to work hardening as expected. Moreover, stress shielding in the immediately surrounding elements is attenuated as the effective stress riser, or notch, is much more diffuse. Effectively, the initial yield stress in the elements associated with the inner HAZ, TMAZ, and nugget is relatively constant. Hence, initial deformation is accommodated by a larger bulk region of elements in the

weld. This, in turn, allows deformation to be accommodated by a progressively wider region, in the elements associated with the HAZ. Generally, the prediction of initial deformation response demonstrates closer correlation with the experimentally measured deformation response, which shows that initial deformation is accommodated over the inner HAZ, TMAZ, and nugget (see §4.0.1).

The results of simulations 6-7 (figure 8b-c) indicate that the upper bound k-parameter distribution is a better approximation to the actual distribution in the weld; the predicted solution has better correlation with experimental observations over the early stages of deformation. From a metallurgical perspective, this may seem illogical because a step function is a purely mathematical construct, unlikely to occur in a continuous system. However, the discrete step changes in properties coincide with locations where rapid variation in the weld microstructure are observed, as described in chapter **??**. These positions relate to the theoretical point where full softening occurs and the position where grain size refinement changes rapidly due to recrystallisation. The former occurs at the interface of the inner and outer HAZ and the latter occurs within the TMAZ, which is an extremely narrow region of the microstructure. When these properties are resolved on a macro structural scale, the property variation is effectively discrete. Thus, it is unsurprising that a step function appears to be representative of the mechanical properties at a macro scale. The definition of element wise constitutive models has enabled a better overall definition of local properties compared to the lumped mass approach, hence, the effects of small variations in the user input property distribution are observable as the effect of intrinsic modelling errors is attenuated. It must be noted that the upper bound k-parameter distribution, by definition, represents an over estimate of the mechanical properties in the weld. However, it is likely that the true k-parameter distribution is closer to the upper bound distribution than to the lower bound.

5.3.3. Non-linear response

Simulations 8-9 are based on the optimal initial yield stress distribution obtained from simulations 5-7. Therefore, yield stress is assumed to vary linearly with hardness, the optimal distribution of hardness is assumed to be diffuse (as in simulation 5), and the optimal k-parameter distribution is stepped (simulation 7). In simulation 8, the plasticity distribution is defined according to the lower bound combination of B and n-parameters; in simulation 9 the upper bound combination is used. It is expected that the whilst initial deformation occurs across the nugget region, due to the inclusion of work hardening properties, strain is accommodated across the HAZ before finally localising in the region associated with the hardness minima on the advancing side of the weld.

However, figure 8d (simulation 8) indicates that initial yielding occurs within the elements associated with the nugget region, and that deformation strain remains confined within the elements associated with the TMAZ and nugget region throughout the entire simulation. At first glance, the reader may have expected a predicted distribution similar to simulation 5 (figure 8a), as the models have the same initial distribution of yield stress. However, the response can be understood by examining the effect of varying the B and n-parameters locally. Figure 10 illustrates the plastic response of the nugget based on the lumped mass assumption and using the upper and lower bound distributions of work hardening response, assuming the same initial yield stress (A-parameter). In the lumped mass approach, the B and n parameter is assumed to be the same as the parent material. In the lower bound approach, the B and n parameter increase smoothly over a narrow region, whereas with the upper bound the parameters increase with a stepped function, effectively over a wider region. The increase in B and n-parameters results in a decrease in the initial post-yield flow stress as a function of plastic strain. Within the weld cross section, the overall decrease in the initial post-yield flow stress is minimised in the lumped mass approach. Using the upper an lower bound distributions, the overall decrease is the same, but greater than the lumped mass assumption. However, the decrease occurs over a narrower region with the lower bound distribution, whereas with the upper bound distribution the decrease occurs rapidly over a wider area.

Hence, the initial post-yield flow stress distribution also acts as a meso-scale stress riser, or notch, in a similar way as the initial yield stress distribution. The stress concentration is much more diffuse using the upper bound distribution and more severe using the lower bound distribution. Thus, the stress concentration induced by lower bound distribution of B and n parameters dominates the initial post-yield response, promoting strain localisation within the weakest elements, i.e. in the centre of the nugget. As a result, the elements of the nugget accommodate all the post-yield deformation strain over the entire simulation. In contrast, due to the constant B and n parameters in the lumped mass method, the initial increase in post-yield flow stress due to work hardening is significantly greater than either the upper or lower bound distributions. Therefore,

using the lumped mass method assumptions, immediately after yielding, the flow stress in the elements associated with the nugget increases sufficiently fast enough to allow the immediately surrounding elements to yield and accommodate deformation strain. Therefore, simulation 8 indicates that the assumption of lower bound distribution of both B and n parameters leads to under prediction of the post-yield work hardening response locally in the weld.

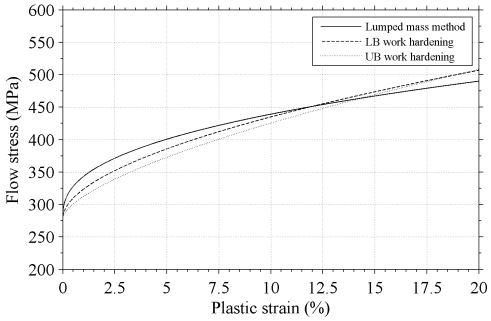

Figure 10: The plastic response of the nugget defined using the same initial yield stress (A-parameter). However, the B and n parameters are based on the lumped mass method, the lower bound distributions, and the upper bound distributions.

In contrast, figure 8e (simulation 9) shows that the predicted evolution of strain distribution correlates much more closely to the expected response. Indeed, it also correlates much more closely to the experimentally measured response (Figure 8g). As mentioned earlier, the step change in the upper bond distribution of B and n parameters associated with the initial post-yield plastic response, induces a meso-scale stress concentration that is more diffuse than the lower bound distribution. This enables more elements associated with the nugget, TMAZ, and inner HAZ to accommodate the initial post-yield deformation strain. As a result, these inner regions can work harden up to the critical point in global deformation. Beyond this critical point, the flow stress of the inner regions of the HAZ, TMAZ, and nugget exceeds the flow stress in the outer HAZ, as illustrated in figure 9. Hence, the overall distribution in flow stress in the outer HAZ, which is linked to the volume fraction of Ω phase, promotes the distribution of strain towards the centre of the weld. However, the mismatch in flow stress at the interface between the inner and outer HAZ, which is linked to the local capacity for work hardening, prevents strain localisation in the centre of the weld. Deformation strain is constrained to localise at the the interface of the inner and outer HAZ, which in 2139-T8 subject to FSW, is coincident with the geometric position of the hardness minima.

It must be noted that the result of simulation 9, by definition, represents an overestimation of the evolution of strain distribution, owing to the user input work hardening response. Thus, there must exist some quantity of error in the prediction, which is evident by direct comparison with the experimentally measured response. However, the predicted results can be considered reliable as they do correlate reasonably well with the experimentally expected results. This result also indicates that the true distribution of work hardening properties in the weld is likely to be closer to the upper bound distribution of work hardening properties. This is a reasonable suggestion because the distribution of mechanical properties lies within the upper and lower bound property distributions, which are based on microstructural and mechanical property based observations of representative weld material. In addition, the result suggests that accurate and reliable estimation of the evolution of strain distribution necessarily requires an accurate description of both the initial yield response, and the work hardening response of the weld. Given that there is correlation between the prediction and experimental measurements, on both a macro and a local scale, the method used to define the local constitutive behaviour can be assumed to be reasonably effective.

5.3.4. Implications for failure prediction

Assuming that the user input property distributions in simulation are both accurate and physically reasonable, the overall methodology must be numerically robust in order to assess the wider implications of its results. Figure 8f shows that the numerical prediction from the mesh resolution study (simulation 10) is both qualitatively and quantitatively similar to figure 8e (simulation 9). Initial yielding occurs within the elements associated with the nugget, TMAZ, and inner HAZ; as the local flow stress increases in these elements via work hardening, progressive yielding occurs in the immediately surrounding elements of the outer HAZ. The characteristic distribution of strain is increasing towards the centre of the weld. The characteristic distribution of strain increases up to a critical point, beyond which, strain begins to localise at the interface between the inner and outer HAZ. In addition, the overall distribution of absolute strain across the weld, and the peak values of strain, are comparable in figure 8e-f. Hence, it can be assumed that sufficient mesh convergence has been achieved, and the prediction is relatively insensitive to mesh size. This indicates that the predictions using the method in simulation 9 are reliable from a numerical perspective.

In light of the numerical stability of the modelling method,

it is likely that the mechanical property distributions across the weld are optimally represented by those used in simulation 9: a smooth distribution of hardness, and a stepped distribution in k, B, and n-parameters. As described previously, the property distributions correlate with the observed microstructural variation across the weld and are justified. The predicted values of directional plastic strain under these optimal user inputs (figure 8e) have reasonable correlation with experiment (figure 8g). As mentioned previously, failure in ductile materials is linked to plastic strain, hence, the optimal model provides a reasonable method for predicting the location of final failure. Indeed, the methodology developed in this chapter has been shown to produce improved prediction of the evolution of geometric strain distribution under uniaxial loading conditions compared to the lumped mass approach.

Whilst a particular failure criterion was not considered in this case, it is likely that the method developed here would provide a more accurate estimate of failure under loading compared to predictions using the lumped mass method, for a given failure criterion. This is because the lumped mass method leads causes numerical perturbations and instabilities when used to model welds with complex mechanical property distributions. In addition, there are numerous examples, in the public domain, of the use of detailed constitutive models in the lumped mass method to improve the reliability of numerical predictions of strain [5, 10, 3]. These models were used to assess the failure performance of welded structures, which is directly linked to the predicted quantity of local plastic strain. Given that the numerical prediction of local strain using the lumped mass approach is dominated by erroneous over-prediction of local strains, the efficacy of improving failure assessments through implementing detailed constitutive models is questionable. The studies in this chapter have shown that a relatively simple Johnson-Cook constitutive model can be used to produce accurate predictions of strain distribution if details of the material microstructure are accounted for. Indeed, the methodology developed here has been shown to produce more reliable predictions of local strain distribution compared to the lumped mass method, and represents an improved approach to assessing structural failure of welds.

5.4. Chapter Summary

In this chapter, the results of a range of numerical studies based on the FEM, which aimed to predict the evolution of local strain distribution in friction stir welded 2139-T8 when loaded in simple uniaxial tension, were presented. The studies utilised a range of methods based on the lumped mass approach, whose application in the public domain is relatively common. In addition, an automated method for implementing complex mechanical property distributions, which are related to characteristic metallurgical properties, into FE based models of welds was described. This method was utilised to systematically study the effects of including details of local initial yield stress and work hardening response. Collectively, the studies indicated that simulations based on the lumped mass method enhanced intrinsic errors in the FEM, and that it could not be used to provide good quantitative correlation, on a local scale, with the experimentally measured strain response. Moreover, the numerical studies using the approach presented here indicate that successful FE based modelling of welds necessarily requires accurate definition of the local distribution of initial local yield stress and work hardening response. In addition, the studies provided an insight into the true nature of the distribution of mechanical properties, which tend to be diffuse in the outer regions of the HAZ, and more discrete in the inner regions of the inner HAZ, TMAZ, and nugget; this observation correlates with microstructural characterisation of the welded described in chapter **??** and the known link between microstructure and mechanical properties. The method presented here represents an improvement in numerical modelling approach, and has the theoretical property of being insensitive to either the loading configuration or geometric scaling. This also represents an improvement over existing lumped mass techniques, however, this property is tested in chapter **??**.

6. Conclusions

In this study, an FE based modelling method, which incorporates element-wise material property variation to detail the strong material property gradients arising from the welding process, was utilised to predict the structural response of FSW 2139-T8 under complex loading configurations, including blast loading. The method requires an understanding of the strengthening mechanism variation in FSW 2139-T8 and is only feasible through automation of the mesh building process. The method utilised removes the need to calibrate models geometry to a particular loading configuration, rather it is calibrated to a normalised weld condition; this removes modelling errors which may arise when extending models to study structural performance under different loading configurations. Moreover, this allows the method to be used to study the effect of welding parameters on structural performance, potentially enabling numerical weld optimisation, which is theoretically applicable to

any heat treatable aluminium alloy. The method has been verified experimentally using DIC for FSW 2139-T8 in under uniaxial tension. The method provides good correlation for strain evolution both globally and locally across the weld zone; this represents an improvement over existing techniques reported in the public domain. Furthermore, strong supporting experimental evidence has been generated which indicates that the method provides good qualitative and quantitative correlation with experimental evidence when extended to more complex loading configurations; this represents an improvement on modelling techniques available in the public domain.

Acknowledgements

The authors acknowledge the funding granted from EPSRC via the Advanced Metallic Systems CDT (EP/L016273/1) at the Universities of Manchester and Sheffield and LATEST2 program (EP/G022402/1). Further, the authors acknowledge DSTL for their contribution towards development of the FE method; Constellium for the provision and manufacture of materials; and Blastech for technical support during blast testing. Thanks also to David Strong and Bill Storrey for their contribution towards experimental testing; and Samuel Tammas-Williams, Tomas Brownsmith, and Richard Watson for their assistance in producing this paper. Please contact the corresponding author for access to the original data used in this article.

References

[1] M. Grujicic, G. Arakere, A. Hariharan, B. Pandurangan, Two-level weld-material homogenization for efficient computational analysis of welded structure blast-survivability, Journal of Materials Engineering and Performance 21 (6) (2011) 786 – 796. doi:10.1007/s11665-011-9876-5.
URL http://www.springerlink.com/index/10.1007/s11665-011-9876-5

[2] B. McWilliams, H. Jian, C. Yen, Numerical simulation and experimental characterization of friction stir welding on thick aluminum alloy AA2139-T8 plates, Materials Science and Engineering: A 585 (2013) 243–252. doi:10.1016/j.msea.2013.07.073.
URL http://linkinghub.elsevier.com/retrieve/pii/S0921509313008435

[3] A. Reis, P. Teixeira, J. Ferreira Duarte, A. Santos, A. Barata da Rocha, A. Fernandes, Tailored welded blanks - an experimental and numerical study in sheet metal forming on the effect of welding, Computers & Structures 82 (17-19) (2004) 1435–1442. doi:10.1016/j.compstruc.2004.03.039.
URL http://linkinghub.elsevier.com/retrieve/pii/S0045794904001294

[4] K. Zhao, B. Chun, J. Lee, Finite element analysis of tailor-welded blanks, Finite Elements in Analysis and Design 37 (2) (2001) 117–130. doi:10.1016/S0168-874X(00)00026-3.
URL http://linkinghub.elsevier.com/retrieve/pii/S0168874X00000263

[5] D. Kim, W. Lee, J. Kim, C. Kim, K. Chung, Formability evaluation of friction stir welded 6111-T4 sheet with respect to joining material direction, International Journal of Mechanical Sciences 52 (4) (2010) 612–625. doi:10.1016/j.ijmecsci.2010.01.001.
URL http://linkinghub.elsevier.com/retrieve/pii/S0020740310000020

[6] M. Grujicic, G. Arakere, A. Hariharan, B. Pandurangan, Two-level weld-material homogenization for efficient computational analysis of welded structure blast-survivability, Journal of Materials Engineering and Performance 21 (June) (2011) 786–796. doi:10.1007/s11665-011-9876-5.
URL http://link.springer.com/10.1007/s11665-011-9876-5

[7] A. Zadpoor, J. Sinke, R. Benedictus, Finite element modeling and failure prediction of friction stir welded blanks, Materials & Design 30 (5) (2009) 1423–1434. doi:10.1016/j.matdes.2008.08.018.
URL http://linkinghub.elsevier.com/retrieve/pii/S0261306908004214

[8] M. Grujicic, G. Arakere, B. Pandurangan, A. Hariharan, C. Yen, B. Cheeseman, Development of a robust and cost-effective friction stir welding process for use in advanced military vehicles, Journal of Materials Engineering and Performance 20 (1) (2010) 11–23. doi:10.1007/s11665-010-9650-0.
URL http://www.springerlink.com/index/10.1007/s11665-010-9650-0

[9] C. Genevois, A. Deschamps, P. Vacher, Comparative study on local and global mechanical properties of 2024 T351, 2024 T6 and 5251 O friction stir welds, Materials Science and Engineering: A 415 (1-2) (2006) 162–170. doi:10.1016/j.msea.2005.09.032.
URL http://linkinghub.elsevier.com/retrieve/pii/S0921509305010695

[10] D. Kim, W. Lee, J. Kim, K. Chung, C. Kim, K. Okamoto, K. Wagoner, R.H .and Chung, Macro-performance evaluation of friction stir welded automotive tailor-welded blank sheets: Part II Formability, International Journal of Solids and Structures 47 (7-8) (2010) 1063–1081. doi:10.1016/j.ijsolstr.2009.12.021.
URL http://linkinghub.elsevier.com/retrieve/pii/S0020768310000053

[11] Y. Sato, S. Park, H. Kokawa, Microstructural factors governing hardness in friction-stir welds of solid-solution-hardened Al alloys, Metallurgical and Materials Transactions A 32 (December) (2001) 3033–3042.

[12] Y. Sato, H. Kokawa, Distribution of tensile property and microstructure in friction stir weld of 6063 aluminum, Metallurgical and Materials Transactions A 32 (December).

[13] J. Hallquist, LS-DYNA theory manual, Tech. Rep. March, Livermore Software Technology Corporation, Livermore, USA (2006).
URL http://www.dynasupport.com/manuals/additional/ls-dyna-theory-manual-2005-beta/at_download/file

[14] C. Rhodes, M. Mahoney, W. Bingel, R. Spurling, C. Bampton, Effects of friction stir welding on microstructure of 7075 aluminum, Scripta Materialia 36 (6) (1997) 69–75. doi:10.1016/S1359-6462(96)00344-2.

[15] M. Mahoney, C. Rhodes, J. Flintoff, R. Spurling, W. Bingel, Properties of friction-stir-welded 7075 T651 aluminum, Metallurgical and Materials Transactions A 29.

[16] C. Genevois, A. Deschamps, A. Denquin, B. Doisneau-Cottignies, Quantitative investigation of precipitation and mechanical behaviour for AA2024 friction stir welds, Acta Materialia 53 (2005) 2447–2458.

doi:10.1016/j.actamat.2005.02.007.

[17] D. Systèmes, Getting started with ABAQUS: Interactive Edition, 2nd Edition, Dassault Systèmes, London, 2010.

[18] W. Chien, J. Pan, P. Friedman, Failure prediction of aluminum laser welded blanks, International Journal of Damage mechanics 12 (2003) 193–233. doi:10.1177/105678903033615.

[19] H. Shercliff, M. Ashby, A process model for age hardening of aluminium alloys - ii applications of the model, Acta Metallurgica 38 (10) (1990) 1803–1812.

[20] H. Shercliff, M. Ashby, A process model for age hardening of aluminium alloys - i. the model, Acta Metallurgica 38 (10) (1990) 1789–1802.

[21] J. Robson, A. Sullivan, Process model for strength of age hardenable aluminium alloy welds, Materials Science and Technology 22 (2) (2006) 146–152. doi:10.1179/174328406X81603.
URL http://openurl.ingenta.com/content/xref?genre=article\&issn=0267-0836\&volume=22\&issue=2\&spage=146

[22] A. Sullivan, C. Derry, J. Robson, I. Horsfall, P. Prangnell, Microstructure simulation and ballistic behaviour of weld zones in friction stir welds in high strength aluminium 7xxx plate, Materials Science and Engineering: A 528 (9) (2011) 3409–3422. doi:10.1016/j.msea.2011.01.019.
URL http://linkinghub.elsevier.com/retrieve/pii/S092150931100027X

[23] M. Peel, A. Steuwer, M. Preuss, P. Withers, Microstructure, mechanical properties and residual stresses as a function of welding speed in aluminium AA5083 friction stir welds, Acta Materialia 51 (16) (2003) 4791–4801. doi:10.1016/S1359-6454(03)00319-7.
URL http://linkinghub.elsevier.com/retrieve/pii/S1359645403003197

[24] K. Jata, S. Semiatin, Continuous dynamic recrystallization during friction stir welding of high strength aluminum alloys, Scripta Materialia 43 (8) (2000) 743–749. doi:10.1016/S1359-6462(00)00480-2.
URL http://linkinghub.elsevier.com/retrieve/pii/S1359646200004802

[25] J. Quinta Da Fonseca, P. Mummery, P. Withers, Full-field strain mapping by optical correlation of micrographs acquired during deformation, Journal of Microscopy 218 (April) (2005) 9–21. doi:10.1111/j.1365-2818.2005.01461.x.

[26] J. Robson, N. Kamp, A. Sullivan, H. Shercliff, Modelling precipitate evolution during friction stir welding of aerospace aluminium alloys, Materials Science Forum 519-521 (2006) 1101–1106. doi:10.4028/www.scientific.net/MSF.519-521.1101.
URL http://www.scientific.net/MSF.519-521.1101